THE JOURNAL OF PHYSICAL CHEMISTRY A
A JOURNAL OF THE AMERICAN CHEMICAL SOCIETY

pubs.acs.org/JPCA

Article

Triple Emission of 5′-(*para*-R-Phenylene)vinylene-2-(2′-hydroxyphenyl)benzoxazole (PVHBO). Part II: Emission from Anions

Joseph J. M. Hurley,[§] Quinton J. Meisner,[§] Peijun Guo, Richard D. Schaller, David J. Gosztola, Gary P. Wiederrecht, and Lei Zhu*

Cite This: *J. Phys. Chem. A* 2022, 126, 1062−1075

Read Online

ACCESS | Metrics & More | Article Recommendations | Supporting Information

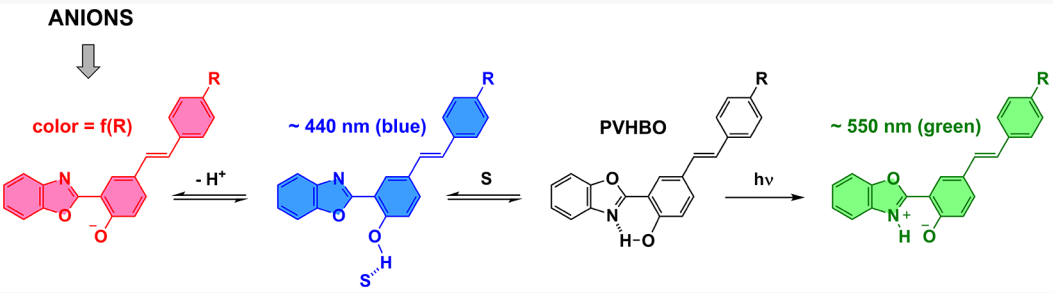

ABSTRACT: This paper is the second part of a study on the effects of a substituted 5′-phenylenevinylene (PV) functionality on the emission properties of 2-(2′-hydroxyphenyl)benzoxazole (HBO)—a dye that is known for excited-state intramolecular proton transfer. The topical compounds are referred to as **PVHBO**s, each of which is a structural fusion of HBO and a 4-hydroxy-4′-R-stilbene fluorophore that occurs at the hydroxyphenyl moiety. Therefore, the resulting fusion fluorophore manifests the properties of one component or the other, as governed by its interactions with the environment. In part I (the preceding paper), **PVHBO**s are divided into two groups depending on whether the R substituent is electron-donating/neutral (group I) or electron-withdrawing (group II). The difference in absorption and emission properties between groups I and II is explained based on observations from spectroscopic experiments (both steady-state and time-resolved) and quantum chemical calculations. In the current paper, the same set of tools is applied to characterize the photophysical properties of the conjugate bases—that is, the anions—of **PVHBO**s. The emission energy of the anion of any group I compound, where the R substituent is either electron-donating or neutral, is situated between those of the neutral enol and keto forms. The emission of the anion of any given group II compound, on the other hand, has a lower energy than both the enol and keto emissions. The frontier molecular orbitals (i.e., HOMO, LUMO, and LUMO + 1) of a **PVHBO** localized on either HBO or stilbenoid are impacted by the substituent R and the solvent/additive differently, which leads to the differences in the optical properties of group I and II **PVHBO**s in both neutral and anion forms.

INTRODUCTION

Fluorophores that tend to undergo excited-state intramolecular proton transfer (ESIPT) offer two emission bands—one from the unaltered molecular structure (normal emission), while the other from the proton-transferred excited-state tautomer (tautomer emission).[1−5] The emissions of the normal and tautomer forms can be tuned to blue and green primary color regions of the visible spectrum, respectively, when an ESIPT core is properly substituted. One class of such compounds is reported in part I of this work (preceding paper),[6] which are ESIPT-capable compounds (2′-hydroxyphenyl)benzoxazoles (HBOs)[7,8] substituted at the 5′-position with *para*-R-phenylenevinylene (**PVHBO**s, Figure 1). **PVHBO**s are fusions of the HBO component and an R-substituted stilbenoid dye. The purpose of the current work is to study how the R group influences the emission of the conjugate base of a **PVHBO** and whether the last primary color, red, could be generated by deprotonation of a **PVHBO**. If that could be done, three primary colors—blue, green, and red—may be materialized using a single fluorophore. Beyond the description of the properties of **PVHBO**s, this work demonstrates the involvement of acid/base chemistry in the ground state as another option to control the emission color of an ESIPT dual-emitting dye. As stated in part I, developing multiple-emission fluorophores is fundamentally challenging and interesting, while products with new and potentially useful properties might be further modified to meet industrial benchmarks as components of organic light-emitting diodes.[9−11] The challenges in the fundamental front and the likelihood of

Received: November 29, 2021
Revised: January 24, 2022
Published: February 10, 2022

https://doi.org/10.1021/acs.jpca.1c10167
J. Phys. Chem. A 2022, 126, 1062−1075

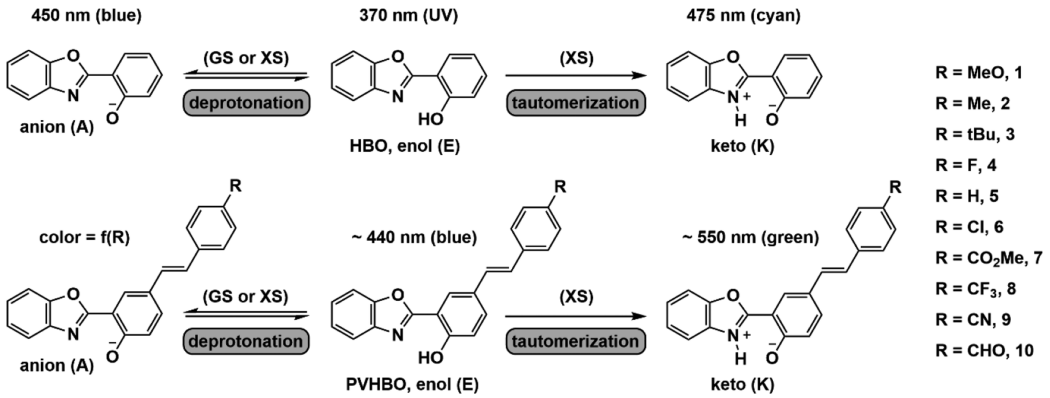

Figure 1. Three emission bands of HBO and 5′-(4-R-phenylenevinylene)HBO (**PVHBO**): enol (E), keto (K), and anion (A). GS = ground state S_0; XS = first excited state S_1. The compounds are numbered in the order of increasing σ_p^+ values of R groups.

new utilities of the finished products have provided the motivation for completing this work.

In part I,[6] we reasoned that in order to develop a dye that emits in three primary colors, a lead fluorophore that is capable of producing three emission bands ought to be identified, based on which structural modifications could be carried out to tune the three bands to primary colors. The lead compound that we selected was HBO, while the structural modification that we elected to execute was the installation of an R-substituted phenylenevinylene (PV) group at the 5′-position (Figure 1). In a solvent not competitive in hydrogen bonding, HBO maintains an intramolecular hydrogen bond (HB), by which the ESIPT occurs to afford the tautomerized dye that emits around 475 nm (i.e., keto emission). The emission of the normal structure centered at ∼370 nm (i.e., enol emission) becomes the major component in a hydrogen bonding-capable solvent because within the solvent/HBO complex the linchpin for ESIPT, which is the intramolecular HB, is no longer present. When the unsubstituted HBO is deprotonated, the emission of the anion is found at 450 nm. Therefore, HBO is able to provide three emission bands that cover from near-UV (enol emission) to cyan color (keto emission). In part I (preceding paper),[6] the enol and keto emissions of the PV-modified HBO molecules (**PVHBO**s) appear in the blue and green regions. In part II, structural factors that would provide a red-emitting anion are determined.

METHODS

The synthesis and characterization of **PVHBO**s were reported in the preceding paper.[6] The spectroscopic and computational procedures are also adopted from those of the preceding paper,[6] in which details were provided. The key points are the following: the steady-state spectral data were collected on a Cary 100 spectrophotometer (absorption) and a Cary Eclipse fluorimeter (emission). The samples were prepared in semiquantitative quartz cuvettes (0.5−1 mL volume and 1 cm path length). The concentrations of the emission samples were such that the absorption at the excitation wavelength was kept at ∼0.1 or lower to minimize the inner filter effect. The picosecond time-resolved emission spectra were measured on a Hamamatsu C5680 streak camera system. The time resolution of the shorter time window was set to 2 ps, while the photons were collected in the longer time window up to 2 ns. The sample concentrations were 50 μM, prepared in a 2 mm path length quartz cuvette. The time-correlated single-photon counting experiments were done on a FluoroMax-4 fluorimeter. The excitation source was a 455 nm light-emitting diode with a repetition rate of 1 MHz. The femtosecond transient absorption (fsTA) spectra were acquired on an Ultrafast Systems transient absorption spectrometer (Helios) with a ∼100 fs temporal resolution (fixed at 130 fs during fitting). Sample preparation procedures were the same as in the streak camera experiments. The quantum chemical calculations were done using the software TURBOMOLE 7.4.[12]

RESULTS

Molecular Design. Fusing HBO and a substituted stilbenoid at the hydroxyphenyl moiety creates the **PVHBO** compounds listed in Figure 1. The difference among these compounds is the electronic nature of the substituent R. As shown in part I,[6] the neutral **PVHBO**s are capable of solvent-modulated ESIPT similar to HBO, namely, two emission bands of a **PVHBO** were observed in a solvent-dependent manner. The keto emission originates from the intramolecularly hydrogen-bonded ground state, while the enol emission results from the excitation of the solvent-hydrogen-bonded **PVHBO** without an intramolecular HB. Unlike HBO, upon deprotonation of a **PVHBO**, these compounds may act similarly to phenolate-containing stilbene fluorophores, a consequence of which would be the appearance of a charge-transfer-type emission from the anion when the R group becomes increasingly e-withdrawing.

Absorption of Anions. Compounds **1**−**10** were deprotonated using the organic base 1,8-diazabicyclo[5.4.0]undec-7-ene (DBU) in dimethyl sulfoxide (DMSO). As an example, the progressive changes in the absorption spectrum upon the addition of DBU up to 30 molar equivalents in a sample of **5** (R = H) are shown in Figure 2. The evolution of the absorption spectrum of **5** during a similar DBU titration experiment in acetonitrile (ACN) is shown in Figure S1. The absorption band at 312 nm decreases as the band at 389 nm increases, correlating with the production of phenolate at the expense of the neutral phenol form. The shift of absorption to a longer wavelength was expected,[13,14] and it is replicated in the rest of the **PVHBO**s. As shown in Figure 3, the anions of the derivatives with more e-withdrawing R-groups (**7**, **9**, and **10**; i.e., group II compounds, as defined in part I[6]) have significantly longer absorption wavelengths, consistent with stronger charge-transfer-type absorption transitions.

In addition to the red shift of absorption maxima of **PVHBO** anions as the R group becomes more e-withdrawing, the spectral line shape of the absorption band also undergoes

https://doi.org/10.1021/acs.jpca.1c10167
J. Phys. Chem. A 2022, 126, 1062−1075

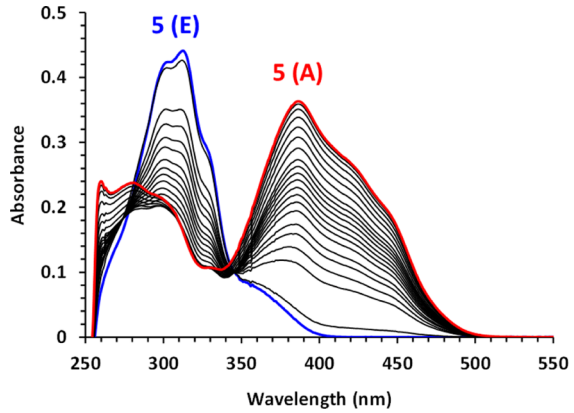

Figure 2. Absorption response of **5** (R = H, 10 μM) in DMSO titrated with DBU up to 30 molar equivalents. E: neutral enol form; A: anion. [DBU] = 0−300 μM (blue to red).

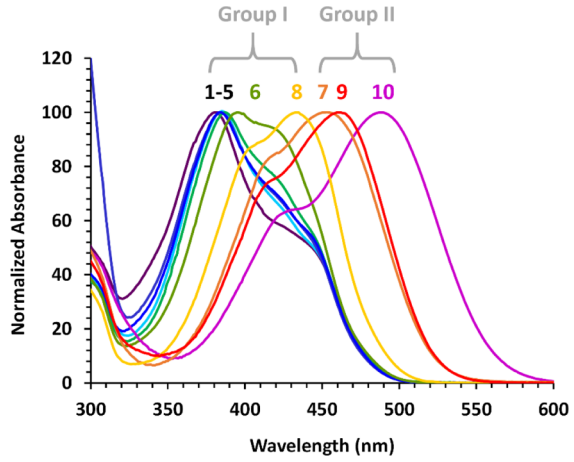

Figure 3. Normalized absorption spectra of the anions of **1**−**10** in DMSO: **1** (R = OMe, violet), **2** (R = Me, navy), **3** (R = *t*Bu, cyan), **4** (R = F, blue), **5** (R = H, green), **6** (R = Cl, yellow-green), **7** (R = CO_2Me, orange), **8** (R = CF_3, yellow), **9** (R = CN, red), and **10** (R = CHO, magenta); [dye] = 10 μM; [DBU] = 30 molar equivalents. The expansion in the group I region is shown in Figure S2.

conspicuous changes (Figure 3). Each of the group I compounds **1**−**5** features a major absorption band with a shoulder on the long wavelength side, while group II compounds **7**, **9**, and **10** have the opposite line shapes where the shoulder is on the short wavelength side of the main band. The absorption line shapes of the deprotonated compounds **6** and **8** appear to be the transitioning cases between groups I and II.

Emission of Anions. The emission spectra of **5** (R = H) in DMSO over the course of the DBU titration are shown in Figure 4a. The 421 nm centered band from the neutral enol form, which is dominant in DMSO in the form of a DMSO−hydrogen-bonded complex,[6] decreases, while a new emission band centered at 504 nm grows as DBU is added. To distinguish the emission of the anion from the keto emission (543 nm) arising from the ESIPT process, the same titration was carried out in ACN (Figure 4b), which showed the decline of the keto band and a similar increase of an emission band at 504 nm. The excitation wavelengths of both titration experiments were selected at the isosbestic points in the absorption mode. Therefore, the increased intensity of emission upon the addition of DBU suggests that the fluorescence quantum yield of the anion is higher than that of the neutral form in both solvents. The normalized emission spectra of the anions of **1** to **10** are shown in Figure 5. The spectra of anions **1**−**6** tightly overlap and maximize at ∼500 nm, while those of **7**−**10** are progressively shifted to longer wavelengths. The anions exhibit sharply different behaviors between the previously classified groups I (**1**−**6** and **8**) and II (**7**, **9**, and **10**).

The group II anions have emission wavelength maxima well past 500 nm, while the emission peaks of group I anions are clustered around 500 nm. These results are recorded in Table 1. The excitation spectra are similar to the absorption spectra (Figure S3). Anions of group II have the longest emission wavelengths with values of 568, 577, and 641 nm for R = CO_2CH_3 (**7**), CN (**9**), and CHO (**10**), respectively. The fluorescence quantum yields of group I anions are found within 0.2−0.3 in DMSO, while those of group II anions (**7**, **9**, and **10**) are higher within 0.3−0.5 (Table 1). These values are larger than those of the neutral forms in DMSO, which are at best measured at 0.11.

Emission Colors and CIE Diagrams. The emission color profiles of the anions of **PVHBO**s in DMSO were mapped on the CIE 1931 XYZ color space (Figure 6). Anions **1**−**6** have CIE 1931 coordinates that cluster in the cyan-teal region, while anions of **7**−**10** follow the curved edge on the outside of the

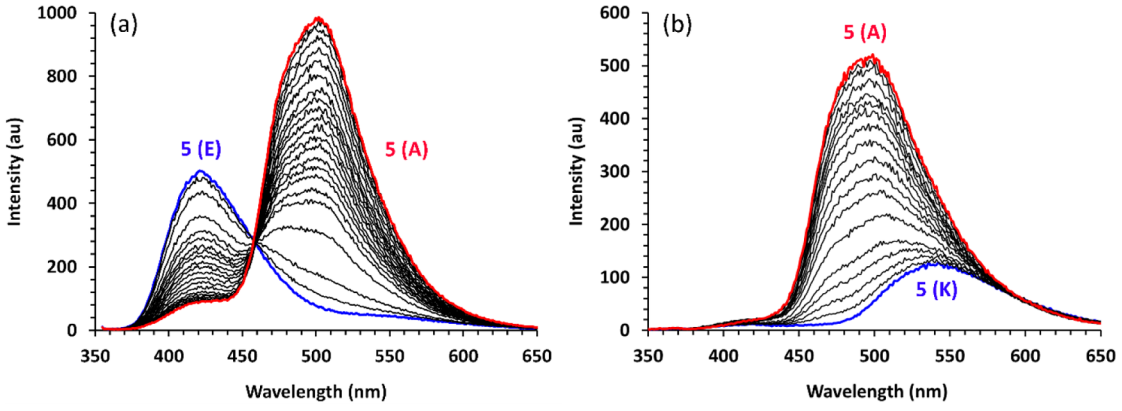

Figure 4. (a) Fluorescence response of **5** (R = H, 10 μM) in DMSO titrated with DBU up to 30 molar equivalents. E: enol; A: anion; K: keto. λ_{ex} = 345 nm; [DBU] = 0−300 μM (blue to red). (b) Fluorescence response of **5** in ACN titrated with DBU up to 100 molar equivalents. λ_{ex} = 332 nm; [DBU] = 0−1000 μM (blue to red).

https://doi.org/10.1021/acs.jpca.1c10167
J. Phys. Chem. A 2022, 126, 1062−1075

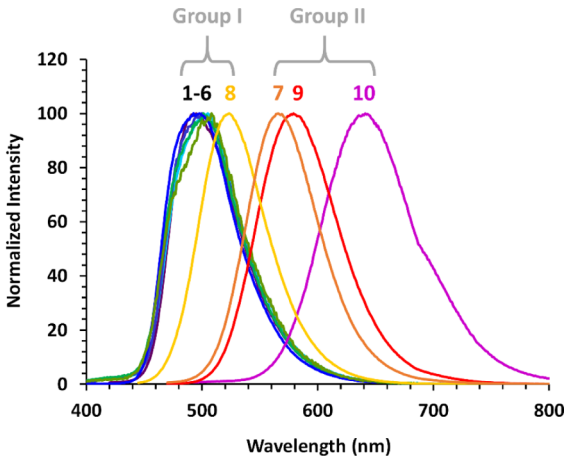

Figure 5. Normalized fluorescence emission spectra of the anions of **1**−**10** in DMSO: **1** (R = OMe, violet), **2** (R = Me, navy), **3** (R = *t*Bu, cyan), **4** (R = F, blue), **5** (R = H, green), **6** (R = Cl, yellow-green), **7** (R = CO_2Me, orange), **8** (R = CF_3, yellow), **9** (R = CN, red), and **10** (R = CHO, magenta); [dye] = 10 μM, [DBU] = 30 molar equivalents, λ_{ex} is varied. The spectra of **1**−**6** closely resemble one another, which makes it difficult to distinguish in this figure.

Table 1. Spectroscopic Properties of the Anions of 1−10 in DMSO[a]

Comp. #	R group	σ_p^+	λ_{abs} (nm)[b]	λ_{em} (nm)	Φ[c]
1	OMe	−0.78	382	495	0.33
2	Me	−0.31	386	500	0.31
3	*t*-Bu	−0.26	386	503	0.29
4	F	−0.07	385	498	0.27
5	H	0	389	504	0.30
6	Cl	0.11	396	508	0.22
7	CO_2CH_3	0.49	454	577	0.52
8	CF_3	0.61	434	523	0.20
9	CN	0.66	463	568	0.33
10	CHO	0.73	490	641	0.35

[a]Group II compounds are shaded. [b]Wavelength of maximal intensity beyond 320 nm. [c]Absolute emission quantum yield.

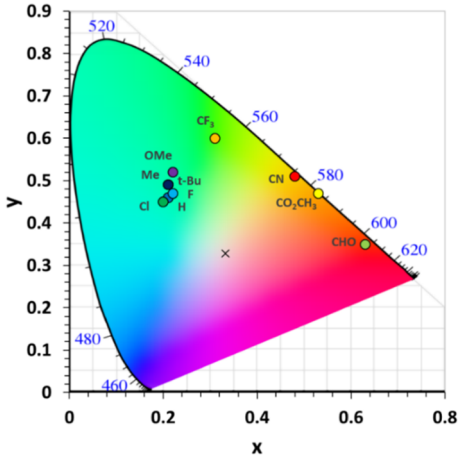

Figure 6. CIE 1931 color space diagram of the anions of **1**−**10** in DMSO. The identities of the R substituents are marked on the graph. White-light reference point: (x,y) = (0.33, 0.33) (×), [dye] = 0.5 μM, [DBU] = 15 μM, λ_{ex} = 370 nm (group I), 450 nm (group II).

coordinate space (i.e., the gamut), indicating that the anions are relatively monochromatic in their emission profile and narrow in their emission bandwidths. The photographs (Figure 7) of the emission of the anions show the difference between members of groups I and II: all group I anions (top row) emit in green, while group II anions (bottom row) emit at longer wavelength regions up to red (i.e., the anion of **10**).

Ultrafast Time-Resolved Emission and Absorption Spectroscopies. The transient emission (TE) and absorption (TA) experiments were done on samples of **PVHBO**s in DMSO in the presence of the organic base DBU (20 molar equivalents). The TE data were collected using a Hamamatsu C5680 streak camera that characterizes the "short" and "long" decays within different time windows. The short time window offers a time resolution at ∼2 ps, while within the long time window photons are captured with a time delay of up to 2 ns. The TA data were acquired on an Ultrafast Systems TA spectrometer (Helios) with a ∼100 fs temporal resolution. The instruments and their setup were identical to those employed and described in the preceding paper.[6]

Time-Resolved Emission. The excitation wavelength was set at 420 nm where only the anions absorb. Each sample was prepared in a 2 mm cuvette with a concentration of 50 μM. For each anion, a single emission band was observed (e.g., see spectra of the anions of **5** and **9** in Figure 8a−d). During the short time window of observations (Figure 8a,c), the emission quickly (<10 ps) reached the maximum intensity and remained constant over the remainder of the observation. No shift of the TE band was observed for anion **5** in either time windows (Figure 8a,b), while a red shift of the emission of anion **9** was discernible but unremarkable (Figure 8d). For the anions of group I compounds **1**−**6**, the maxima of the emission bands were found to overlap at ∼ 510 nm. For anions of **7**−**9** that contain e-withdrawing substituents, the emission band appeared in longer wavelength regions. The anion of **8** (group I) peaked at 535 nm, while the maxima of the anions of **7** and **9** (group II) were found at ∼580 nm. The values of the emission maxima measured in the TE experiments were similar to those recorded during steady-state measurements (Table 1).

The collected time constants of the **PVHBO** anions are listed in Table S1. The values of the rise time t_1 were extracted from track 1 data with a temporal resolution of 2 ps. Based on the profiles of the time-dependent photon counts (Figure S4), there appear to be a slower, low-amplitude rise on the scale of tens of picoseconds. However, fitting for this component was not successful. The values of t_2 and t_3 were fitted from track 4 measurements with a longer time window up to 2 ns. The rise of the emission (t_1) mostly occurred within 5 ps, which is close to the instrument response. Consequently, it would have masked any processes that had occurred prior to this point. The time-dependent traces from track 1 measurements were similar across all anions of the **PVHBO**s (Figure S4), suggesting that either similar photophysical events took place during the short time window, or the time resolution was not high enough to distinguish the initial fast events among the **PVHBO**s.

The t_2 values of all compounds are in the range of hundreds of ps. The amplitudes of t_2 of group II anions (and that of anion of **8**) are larger than those of group I anions. For all anions, there is an additional decay component (t_3 in Table S1) that is longer than 2 ns (except for anion **8** with a t_3 of 0.9 ns), which is the duration of track 4 measurements. For several anions, t_3 values are too long to fit. Those include anions **1** (t_3 ∼ 8 ns), **4**, **5**, and **7**, whose t_3 values are marked as infinity (∞). The abundances of the t_3 component of group I anions

https://doi.org/10.1021/acs.jpca.1c10167
J. Phys. Chem. A 2022, 126, 1062−1075

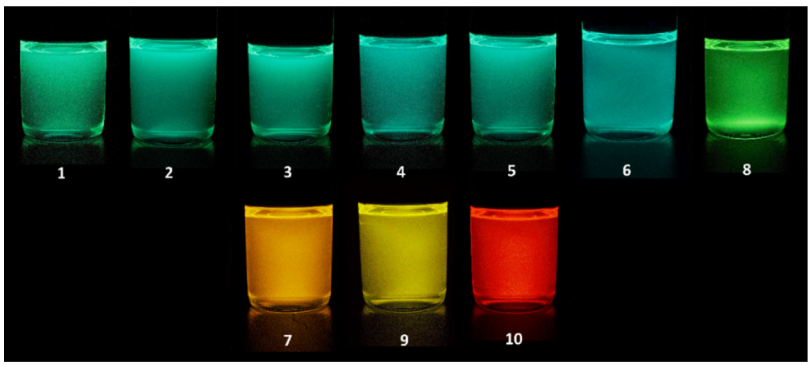

Figure 7. Photographs of **PVHBO** anions in DMSO irradiated using a handheld UV lamp (λ_{ex} = 365 nm). Top: group I; bottom: group II; [dye] ~ 60 μM.

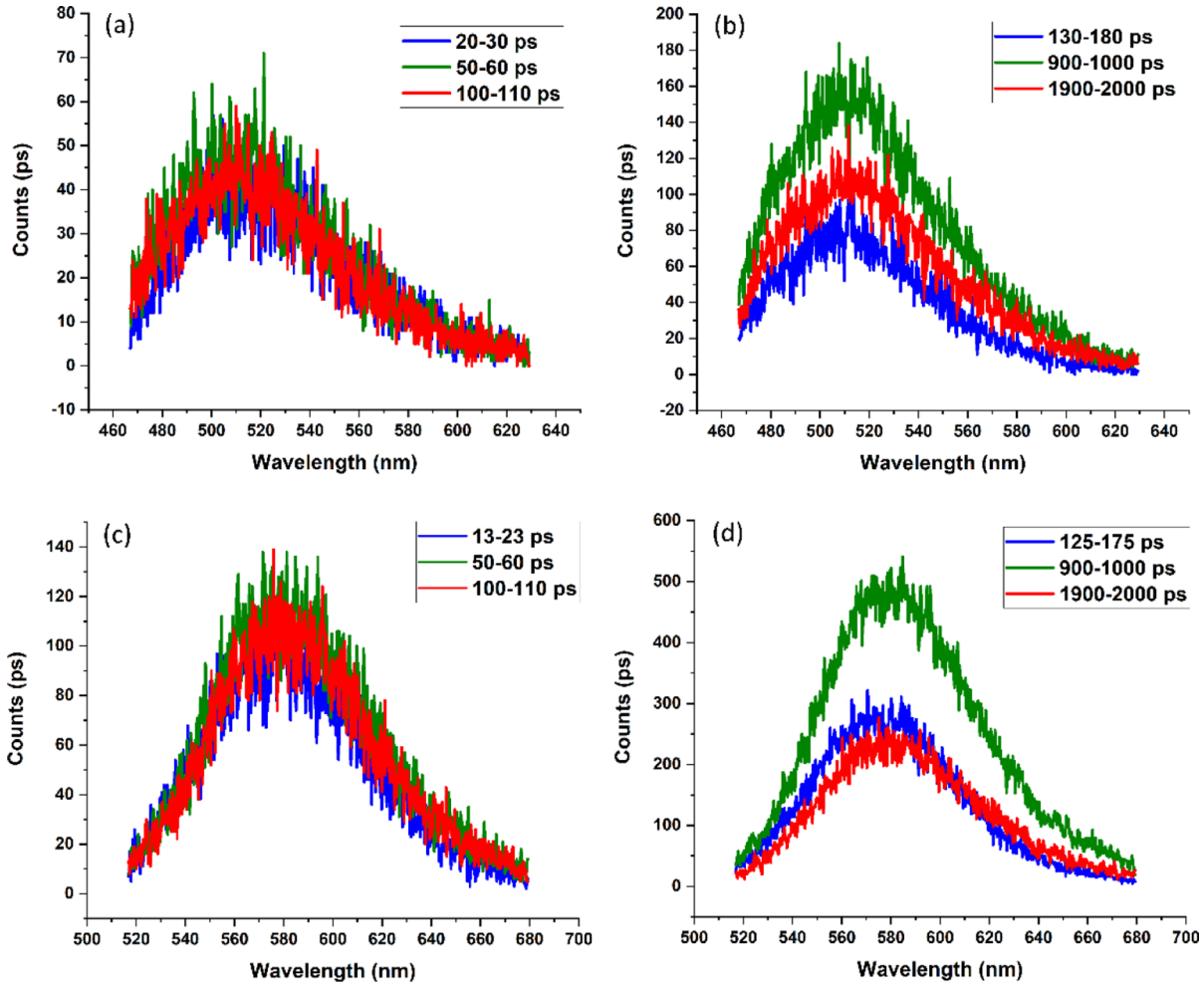

Figure 8. Emission spectra of the anions of **5** (R = H, a,b) and **9** (R = CN, c,d) taken at different time slices. λ_{ex} = 420 nm. [Dye] = 50 μM; DBU = 1 mM.

remain unchanged as the monitoring emission wavelength increases, while those of group II anions become slightly larger as the emission wavelength increases (see the decay of anions **5** and **9** at different wavelength slices in Figure S5, Table S2). The overall decay of the **PVHBO** anions observed at respective wavelengths of maximum intensity is shown in their normalized forms in Figure 9. The traces of the anions of **1**−**5**, all group I members, closely resemble one another. In comparison, the group II anions **7** and **9** show a faster decay in the later stages. The anions of **6** and **8** appear to show behaviors that break the trend—the longest components (t_3) of which are shorter than either of group I or II anions. The fluorescence lifetimes of selected anions (**1**, **5**, **7**, and **9**) were also measured using the time-correlated single photon counting technique. The single-exponential decay model is sufficient for fitting the decay curves, of which the group I anions **1** and **5** have larger time constants than group II anions **7** and **9** (Table S3). This observation is consistent with the overall slower decay of group I anions (**1**−**5**) than the rest that were registered on the streak camera (see Figure 9). As an

https://doi.org/10.1021/acs.jpca.1c10167
J. Phys. Chem. A 2022, 126, 1062−1075

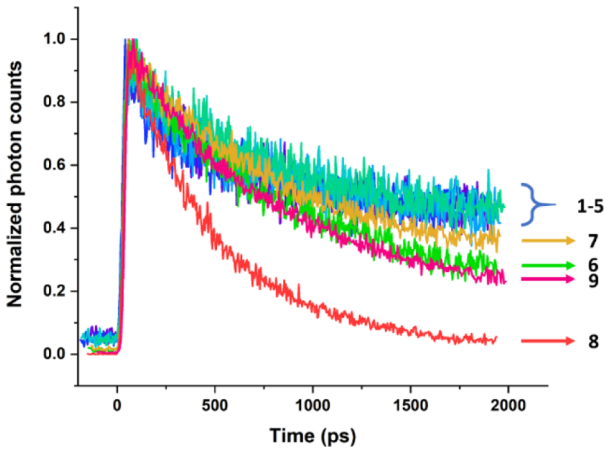

Figure 9. Normalized decay of anion emission bands of **1**−**9** in DMSO monitored using a streak camera at wavelength slices covering the maximum intensity. λ_{ex} = 420 nm; [dye] = 50 μM; [DBU] = 1 mM was used for deprotonation.

example of insensitivity to O_2, the decay trace of the anion of **1** (R = OMe) was not affected by saturating the sample with either nitrogen or compressed air (Figure S6).

Time-Resolved Absorption. The anions of **PVHBOs** (50 μM) were produced by the addition of 20 molar equivalents of DBU to the sample solutions in DMSO. The fsTA data were generated from exciting the samples at 420 nm where only the anions absorb. The experimental details of the fsTA experiments are described in the preceding paper.[6] Group I and II anions show differences in both fsTA spectra and kinetics. Anions of **5** (R = H) and **7** (R = CO_2Me) are used as examples of group I and II members, respectively, for describing these differences.

In the first 200 fs of the fsTA experiment of anion **5** (gray, violet, and blue traces in Figure 10a), a sharp negative peak at ∼470 nm was observed, as well as a positive TA band on the higher energy side which is cut off at 450 nm. The negative spike at ∼470 nm is assigned to the stimulated Raman amplification from the solvent, based on its wavelength and ultrafast response similar to the instrument response (see the blue line, Figure 10c).[15,16] These features are replaced by a new TA band near 450 nm and a relatively broad negative band centered at 500 nm, the latter of which is the stimulated emission (SE) of the anion. These two main features are referred to as blue and middle bands, respectively, according to the convention that is established in the preceding paper.[6] The fsTA spectrokinetic data of anion **5** are shown in Figure S7a as

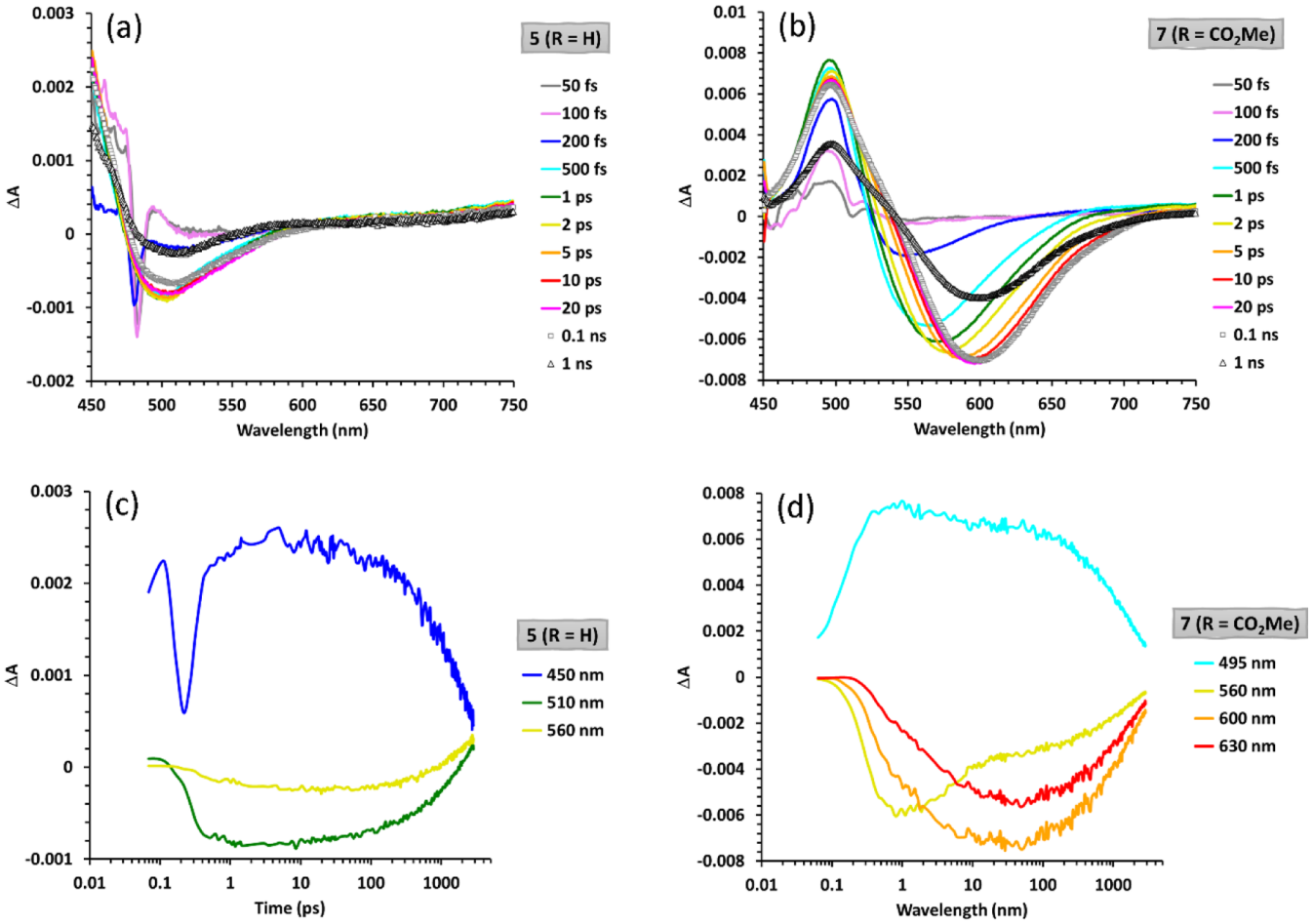

Figure 10. fsTA spectra (a,b) and decay traces (c,d) of the anions of **5** (50 μM, a,c), and **7** (50 μM, b,d). [DBU] = 1 mM. λ_{ex} = 420 nm. Most of the TA spectra are selected from the early stage of decay (50 fs—gray; 100 fs—violet; 200 fs—blue; 500 fs—cyan; 1 ps—green; 2 ps—yellow; 5 ps—orange; 10 ps—red; and 20 ps—magenta). The spectra taken at 0.1 ns (gray squares) and 1 ns (black triangles) are included as examples of those of later stages of decay. The kinetic traces (450 nm—blue; 495 nm—cyan; 510 nm—green; 560 nm—yellow; 600 nm—orange; and 630 nm—red) are plotted on a logarithmic time scale, so that the features from femtoseconds to nanoseconds are displayed.

https://doi.org/10.1021/acs.jpca.1c10167
J. Phys. Chem. A 2022, 126, 1062−1075

a color-annotated contour plot. The TA spectrum of anion **5** rapidly stabilizes after 500 fs, from which point onward up to 100 ps little change was detected (Figure 10a). No time-dependent shifts of any peak maxima (or minima) were observed.

The fsTA of anion **7**, which represents group II compounds, affords relatively strong and well-formed TA bands before the 200 fs mark (blue trace, Figure 10b). The positive blue band, which is an excited-state absorption (ESA), decreases at 500 nm, while the negative middle SE band starting at ∼550 nm eventually shifts to 600 nm over time. The wavelength maximum of the middle SE band red-shifts over a 10 ps span, in contrast to the blue ESA band for which no significant wavelength shift was observed. The kinetic traces plotted in Figure 10d contrast the decay of anion **5** (Figure 10c) in two aspects: (1) the stimulated Raman amplification band close to time zero that appears in the decay traces of anion **5** is obscured in the traces of anion **7**, which has an overall higher TA intensity than anion **5** and (2) the red shift of the middle SE band occurs in anion **7** but not in **5**.

Both the blue ESA and middle SE bands of the anions of group II compounds are red-shifted from those of group I anions (see the difference between Figure 10a,b). This level of difference between groups I and II was not observed in the fsTA spectra of the neutral forms. Among all the features found in the fsTA spectra of neutral and anion forms, only the middle SE bands of group II anions show a noticeable dynamic Stokes shift. This shift that occurs primarily over the first 10 ps was not captured in the TE experiments, which offer a lower time-resolution.

The kinetic traces of the blue ESA and middle SE bands were fit with multiexponential functions to yield the decay time constants (Tables S3 and S4). Three example fits of the blue ESA bands are shown in Figure S8. The picosecond and sub-picosecond time constants t_1 and t_2 of the blue bands of anions **1**−**6** (anions) are not fit with high confidence because the main feature in those decays during the early stage is the stimulated Raman amplification (e.g., see the blue trace in Figure 10c), which cannot be fit by a multiexponential function but has a temporal response comparable to the instrument response. The traces of anions **7**−**9** that contain e-withdrawing substituents produce two short time constants. The rise components (t_1) that are 200 fs or shorter are close to the instrument response function (130 fs). Therefore, they are assigned to the direct excitations of the anions. The t_2 values of **7** and **9** account for the dynamic Stokes shifts within the first ∼10 ps. A t_2 of a similar magnitude was fit from the decay of any group I anion, although without a dynamic Stokes shift. The longest time constants t_3 of almost all anions are in the range of 1−2 ns. The value of t_3 decreases as the anions transition to group II. At the same time, the residual amplitude (y_0) disappears, suggesting an overall faster restoration of group II anions than group I anions to the ground state.

The decay of the middle bands (Table S4) that are primarily accounted for by the SE can be divided into four segments: a sub-picosecond t_1 within 0.1−0.2 ps for describing the rapid formation of the anion emitter, a single picosecond t_2 component of vibrational relaxation, a tens of picosecond component to account for solvent-involved relaxation and perhaps a relatively short-lived excited state, and a nanosecond component for emission. Note that the t_2 components for **7**−**9** have amplitudes generally 1 order of magnitude larger than the other compounds, consistent with the appearance of dynamic Stokes shifts in group II compounds. A residual amplitude is needed for achieving a satisfactory fitting of the middle band, suggesting the presence of either a long-lived excited state or a new species resulted from photobleaching. If the values of two adjacent time constants are similar, or if the amplitude of one component is rather small, they could be merged with the adjacent component to still result in a satisfactory fit. For example, the t_2 components of anions **4** or **8** (0.6 and 0.7 ps, respectively, in Table S4) account for both the initial formation of the SE band and the vibrational relaxation process. The t_3 values of the anions of **7**−**9** are found within 8−10 ps (Table S4), which coincide with the red shifts of the SE bands. The longest t_4 component (in nanoseconds) of the middle SE band matches with the counterpart from the fitting of the blue ESA band, both of which are assigned to the radiative decay of the anion excited state.

Computational Studies. The methods of computation are kept consistent with the ones described in the preceding paper.[6] The ground state of a **PVHBO** anion has two conformational minima in respect of the C−C bond between benzoxazole and phenoxide moieties (Figure S9). In one, the phenoxide is "*cis*" to the azole nitrogen, while in the other, the phenoxide is "*trans*" to the same atom (Figure 11). These

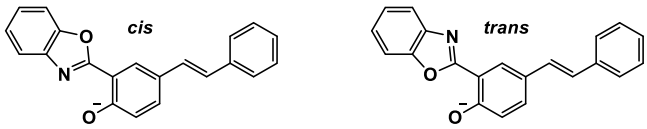

Figure 11. trans and cis conformers of anion **5** (R = H). The optimized structures in both ground and excited (S_1) states are coplanar (see the dihedral angle scan in Figure S9). The trans conformer is 0.2 kcal/mol more stable in the ground state (DFT/B3LYP/def2-TZVPD), while it is 1.8 kcal/mol more stable than the cis conformer in the first excited state (TDDFT/B3LYP/def2-TZVPD).

stereochemical definitions are consistent with those of neutral *cis*- or *trans*-enol forms of HBO.[7] Both conformers of the anion of **5** (R = H) were optimized at the DFT/B3LYP/def2-TZVPD level of theory using the COSMO model to mimic a solvent environment of DMSO (ε = 47). The diffusion function was added in the basis sets to account for the charge in the structure. The trans isomer is slightly more stable (by 0.2 kcal/mol) than the cis isomer. The first two electronic transitions of the two conformers are similar in both excitation energy and oscillator strength (Table S5). For this reason, only the trans isomers of the **PVHBO** anions are computed, and the data from which are listed in this subsection.

The ground-state (S_0) geometries of anions **1**−**10** were optimized at the DFT/B3LYP/def2-TZVPD level of theory, while the COSMO model was applied to account for solvation in DMSO. The excitation energy values of the first two excited states (S_1 and S_2) and their respective oscillator strengths, calculated at the relaxed S_0 geometries, are listed in Table 2. The major contributors to S_1 and S_2 are HOMO → LUMO and HOMO → LUMO + 1 transitions, respectively, across the entire series of compounds. As the R group becomes more e-withdrawing, LUMO and LUMO + 1 start to switch the molecular spaces they occupy. As exemplified in Figure 12, the LUMO of anion **1** (R = MeO) is found on the HBO moiety while the LUM O + 1 resides on the stilbenoid, whereas in anion **9** (R = CN), the LUMO and LUMO + 1 almost entirely

https://doi.org/10.1021/acs.jpca.1c10167
J. Phys. Chem. A 2022, 126, 1062−1075

Table 2. Two Calculated Lowest Energy Electronic Transitions (λ_1 and λ_2 in nm), Oscillator Strengths (f), Dominant MO Contributions at the Optimized Ground State (S_0) Geometries (trans Conformation) of the Anions of PVHBOs, and the Gaps between Their S_1 and S_2 States (ΔE in eV)[a]

Comp. #	R	λ_1 (nm)/f_1	S_1 dom. Contr.[b]	λ_2 (nm)/f_2	S_2 dom. Contr.[b]	ΔE (eV)
1	MeO	428/0.51	H → L, 96%	394/0.95	H → L + 1, 95%	0.25
2	Me	424/0.62	H → L, 98%	393/0.92	H → L + 1, 97%	0.23
3	*t*Bu	424/0.67	H → L, 98%	396/0.89	H → L + 1, 97%	0.21
4	F	421/0.67	H → L, 96%	395/0.71	H → L + 1, 95%	0.19
5	H	420/0.76	H → L, 82%	396/0.72	H → L + 1, 81%	0.18
6	Cl	425/1.04	H → L, 63%	403/0.47	H → L + 1, 63%	0.16
7	CO_2Me	475/1.32	H → L, 96%	405/0.26	H → L + 1, 96%	0.45
8	CF_3	437/1.25	H → L, 88%	403/0.26	H → L + 1, 87%	0.24
9	CN	473/1.35	H → L, 96%	403/0.26	H → L + 1, 96%	0.46
10	CHO	519/1.25	H → L, 98%	403/0.28	H → L + 1, 97%	0.69

[a](TD)DFT/B3LYP/def2-TZVPD level of theory. Solvation is considered using COSMO (ε = 47, DMSO). [b]H—HOMO; L—LUMO; L1—LUMO + 1.

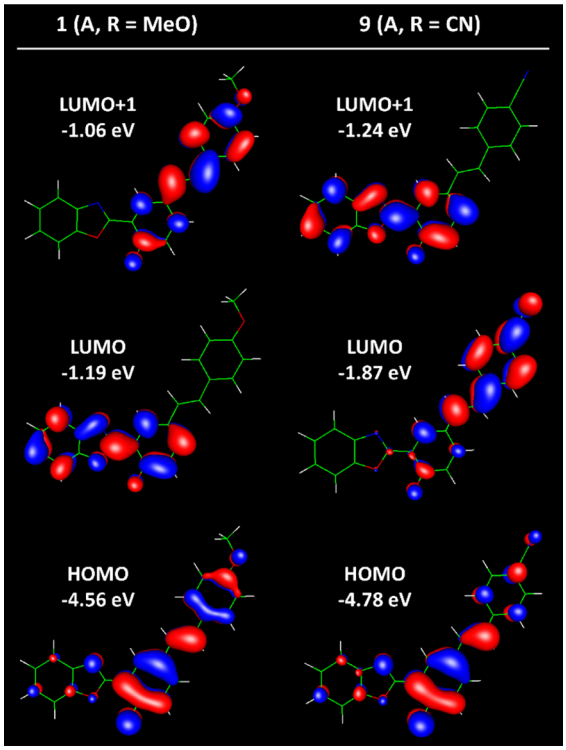

Figure 12. Frontier molecular orbital (FMO) diagrams of the anion (A) forms of **1** (left) and **9** (right) calculated at the DFT/B3LYP/def2-TZVPD level of theory, while solvation is considered using the COSMO model (ε = 47, DMSO). The relative orbital energy values are listed.

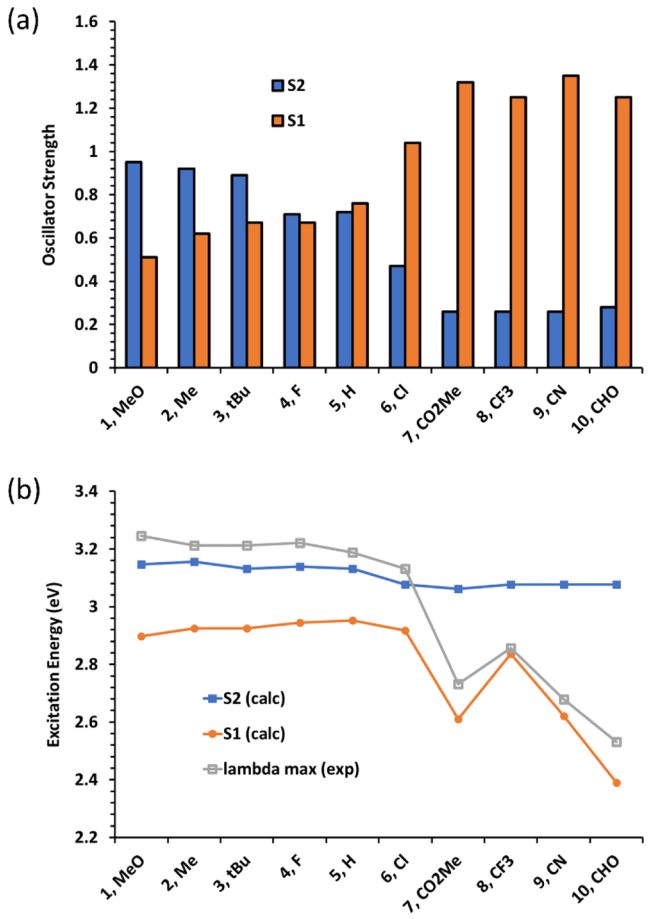

Figure 13. (a) Calculated oscillator strengths of S_1 (orange) and S_2 (blue) states; (b) calculated excitation energies of S_1 (orange filled circles) and S_2 (blue filled squares) at relaxed S_0 geometries, and the experimentally observed absorption maxima (gray open squares).

switch their places. Based on the substituent-dependent energetic order of LUMO and LUMO + 1, the observed energies and the oscillator strengths of the absorption bands can be explained.

The calculated oscillator strength values are plotted in Figure 13a. The S_1 oscillator strength (orange) increases as the R group becomes more e-withdrawing, while the S_2 oscillator strength (blue) wanes. The former is an indicator of the transition probability of the HOMO → LUMO transition, which increases as the LUMO shifts from the HBO moiety to the stilbenoid that overlaps better with the HOMO. At the same time, the HOMO → LUMO + 1 transition becomes less allowed as the LUMO + 1 moves away from stilbenoid toward the HBO moiety, as the R substituent turns more e-withdrawing. The change in the relative oscillator strengths of S_1 and S_2 across the series leads to the switch of the stronger absorption from S_2 to S_1. The calculated absorption energies also match well with the experimentally measured values (λ_{max} in eV in Figure 13b) and spectral line shapes of absorption bands. For anions **1**−**6**, the experimental λ_{max} values track closely with the calculated excitation energy to the S_2 states, when the S_2 states have relatively large oscillator strengths. For

https://doi.org/10.1021/acs.jpca.1c10167
J. Phys. Chem. A 2022, 126, 1062−1075

anions **7**−**10**, the calculated excitation energies of S_1 states are more aligned with the experimental λ_{max} values because the S_1 transition has become more allowed than the S_2 transition based on the calculated oscillator strengths.

The excited-state (S_1) geometries of the **PVHBO** anions are optimized at the TDDFT/B3LYP/def2-SVPD level of theory in vacuum. Compared to the ground-state optimizations, a smaller basis set is selected for the purpose of saving computational cost. The single-point excitation energies are calculated at the relaxed S_1 geometries at the ADC(2)/def2-SVPD level of theory, while solvation is considered with COSMO. The data are listed in Table 3. Larger deviations from the experimental emission maxima relative to the ground-state calculations are expected considering the complications faced by excited-state anion calculations.[14] The excitation energies of anions **1**−**6** are similar between one another and are overestimated from the experimental emission maxima, while those of anions **7**−**10** are progressively lower and are underestimated from the experimental values. The correlation between the R group and the excitation energy reproduces that of the experimental trend (Figure S9), in which the group I anions emit within a narrow region of relatively short wavelengths, while the emission bands of group II anions shift progressively to the red as the R group becomes more e-withdrawing.

Table 3. Calculated Lowest Excitation Energy (λ in nm), Oscillator Strength (f), and the Dominant MO Contribution at the Optimized S_1 Excited-State Geometries (trans Conformation)[a]

Comp. #	R	λ (nm)	f	S_1 dom. Contr.[b]
1	MeO	446	0.45	H → L, 82%
2	Me	469	0.48	H → L, 80%
3	*t*Bu	452	0.53	H → L, 81%
4	F	440	0.46	H → L, 84%
5	H	455	0.53	H → L, 82%
6	Cl	438	0.50	H → L, 84%
7	CO_2Me	743	0.72	H → L, 89%
8	CF_3	602	0.81	H → L, 89%
9	CN	694	0.79	H → L, 88%
10	CHO	918	0.57	H → L, 90%

[a]TDDFT/B3LYP/def2-SVPD level of theory for optimization; PTED-COSMO-ADC(2)/def2-SVPD for single-point excitation energy calculation at the optimized S_1 geometry. Solvation was considered using COSMO (ε = 47, DMSO). [b]H—HOMO; L—LUMO.

The HOMO → LUMO transition is the major contributor to the $S_0 \rightarrow S_1$ excitation at the relaxed S_1 geometry (i.e., emission, Table 3). The HOMO and LUMO plots of the excited anions of **1** (**1a***) and **9** (**9a***), which represent group I and II anions, respectively, are shown in Figure 14a,b. The HOMO and LUMO of **1a*** occupy the stilbenoid and HBO respectively, while those of **9a*** take up almost the opposite physical residence. Neither the LUMO of **1a*** nor the HOMO of **9a*** involves much of the R substituent, while the LUMO of **9a*** almost entirely localizes on the vinylbenzonitrile moiety (Figure 14b). The HOMO of **1a*** is more delocalized on the stilbenoid, within which the phenoxide is favored (Figure 14a). It is therefore reasonable to conclude that the emission of a group II anion is more sensitive to the substituent R than a group I anion based on the observation that out of the four FMOs shown in Figure 14, the substituent R is most involved in the LUMO of **9a***.

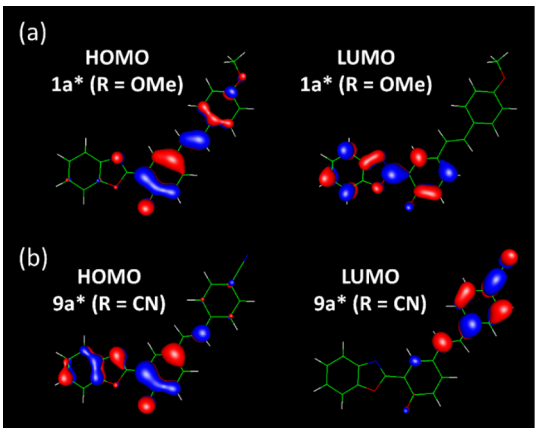

Figure 14. HOMO and LUMO of anions of **1** (**1a***, a) and **9** (**9a***, b) at the relaxed excited-state geometries calculated at the DFT/B3LYP/def2-SVPD level of theory while solvation is considered using the COSMO model (ε = 47, DMSO).

DISCUSSION

Anions of ESIPT Fluorophores. HBO and other ESIPT derivatives have been employed extensively in developing fluorescent probes in biosensing and imaging applications.[17] The dual emission of anion and keto of an ESIPT dye, rather than the more commonly assumed dual emission of enol and keto, has been leveraged for ratiometric sensing.[18,19] Although anions are major emitters of several classes of fluorophores,[14] the photophysical properties of fluorescent anions have not been described as extensively as neutral compounds. Regarding ESIPT-capable fluorophores, one may find works on neutral species more readily than those on anions, which have occasionally been misidentified in the interpretation of anomalous emission bands in the study of neutral species. One of the earliest reports on the anion form of an ESIPT fluorophore is found in a series of publications on 3-hydroxyflavone (Figure 15) by Kasha and coworkers. 3HF is prone to solvent-assisted deprotonation (e.g., by water[20] or formamide[21]). The emission of the anion of 3HF was originally attributed to another form of the excited tautomer of the neutral 3HF.[20,22] Much effort, and years had gone by before the elusive proton transfer-driven photophysics of 3HF was clarified,[20,21] and from the study on 3HF, one may appreciate that the spectroscopic interpretations of ESIPT compounds could be fraught with interference by strongly interacting solvents and other impurities, and they require the utmost attention to detail and rigorous control experiments to test all alternative possibilities to avoid misinterpretations.

Tinuvin P (Figure 15) is a highly photostable compound that is used as a UV light-absorbing additive to polymers. The photostability is attributed to the non-radiative decay of the excited state via ESIPT. The degradation of Tinuvin P over a long period of time, however, was postulated to originate from the photochemistry of the solvent adduct of the compound via an intermolecular HB, which undergoes excited-state deprotonation to afford an excited anion. Through this study, the absorption and emission of the Tinuvin P anion were characterized.[23] Similar to Tinuvin P, aloesaponarin I (AS1 in Figure 15) is a UV-protective component of the aloe extract, which derives its photostability from its ESIPT capacity.[24] The

https://doi.org/10.1021/acs.jpca.1c10167
J. Phys. Chem. A 2022, 126, 1062−1075

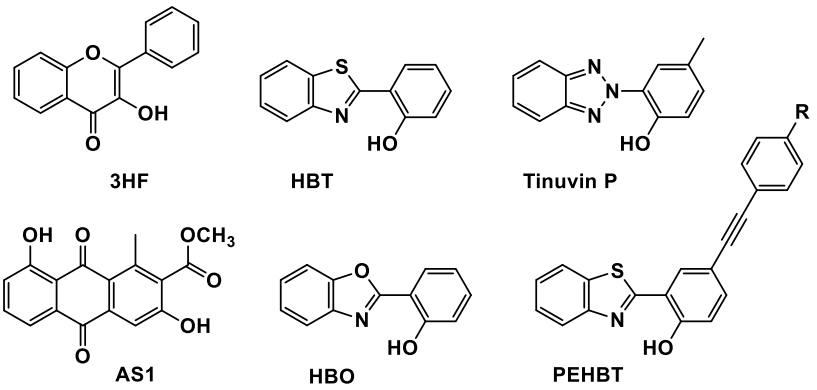

Figure 15. A few ESIPT fluorophores whose properties of anions were reported in literature.

anion of AS1 showed an emission band with longer wavelengths than the emissions of both the normal and proton-transferred tautomer.[24] The deprotonated AS1 was also found to be less photostable than its neutral form and is therefore employed to engage in various photodegradation pathways.

Over the course of studies on HBO by multiple groups, an anomalous long-wavelength absorption band had been noted and attributed to different species. It was later characterized as either the anion or a metal complex of the anion, which could be accidentally produced in strong HB basic solvents.[8] Similar anion chemistry was earlier characterized for 2-(2′-hydroxyphenyl)thiazole (HBT, Figure 15),[25] a compound that differs from HBO by a single atom. As the last example, phenyleneethynylene-substituted HBT (PEHBT, Figure 15) in polar solvents such as MeOH and DMF exhibit a long absorption band, which was characterized as that of the anion.[26] These are the several examples of anions of ESIPT fluorophores that are relevant to the current study.

Absorption. The absorption and emission properties of the anions of **1**−**10** can be explained based on the computed data. Each anion can be considered as a fusion of two chromophores—HBO and stilbenoid—both in deprotonated forms. The absorption spectra of the anions shown in Figure 3 are dominated by the S_1 and S_2 states of each structure. These two states primarily consist of (>80% except anion **6**, see Table 2) the transitions from the HOMO on the stilbenoid to the unoccupied molecular orbitals (LUMO or LUMO + 1) on either HBO or stilbenoid (see examples in Figure 12). For most group I anions (e.g., **1**−**5**), the S_2 state (involving LUMO +1 on stilbenoid) is more allowed than the S_1 state (involving LUMO on benzoxazole), while for group II anions (e.g., **7** and **9**), the S_2 becomes less allowed than the S_1 (Figure 13a), because of the switch in the energy of unoccupied molecular orbitals residing on benzoxazole (LUMOs in group I) and stilbenoid (LUMOs in group II) as the R group becomes more e-withdrawing.

The absorption spectral maxima of group I anions **1**−**5** are insensitive to the R group, while those of a group II anion drop quite readily as the substituent R becomes more e-withdrawing. This difference in the level of absorption sensitivity to the R group may be rooted in the dependence, or otherwise, of FMOs on the R group (Figure 16a). The HOMO energies of all anions are confined in the narrow range of −4.8 to −4.5 eV (blue circles in Figure 16a). The energies of LUMO (−1.2 to −1.3 eV) and LUMO + 1 (−1.1 to −1.2 eV) of group I anions **1**−**6** are close to one another in addition to being insensitive to

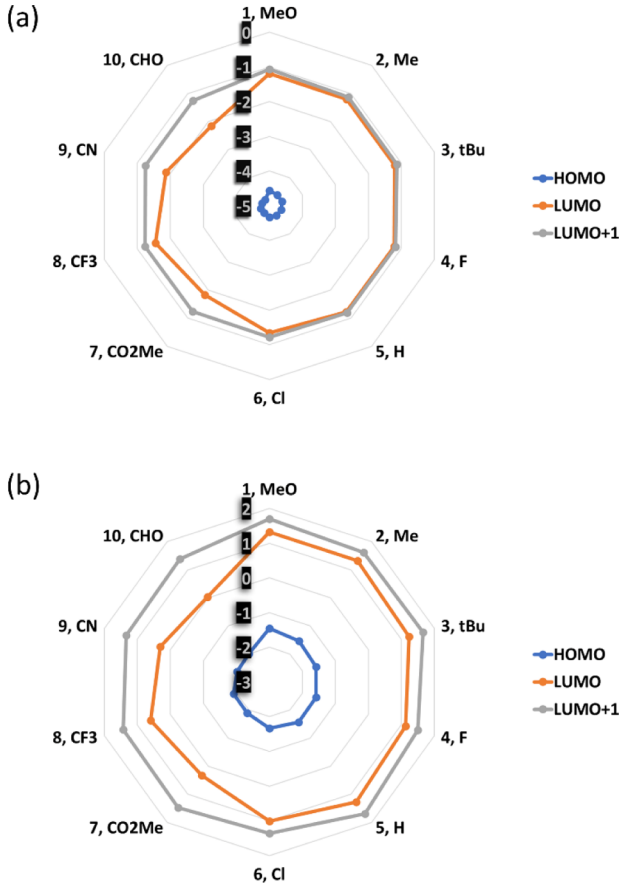

Figure 16. Calculated FMO energies in eV ((TD)DFT/B3LYP/def2-TZVPD) of anions **1**−**10** displayed in radar charts at S_0 (a) and S_1 (b) geometries. The scales in eV are shaded.

the identity of R (right hemisphere of the radar plot in Figure 16a). The closeness between LUMO and LUMO + 1 in anions **1**−**6** suggests that the S_1 (principally HOMO → LUMO transition) and S_2 (principally HOMO → LUMO + 1 transition) states are coasting on the edge of a "phase transition", and foretells a rather dramatic change of behavior as the R group becomes further e-withdrawing. The LUMO level of an anion carrying an e-withdrawing group (**7**−**10**) is noticeably lower than the former group (**1**−**6**) and decreases (except for **8**) as the R group increases on the Hammett scale. The analysis of the correlations of FMO energies to the R group offers a good explanation to the key features of experimentally observed absorption spectra—namely, the

https://doi.org/10.1021/acs.jpca.1c10167
J. Phys. Chem. A 2022, 126, 1062−1075

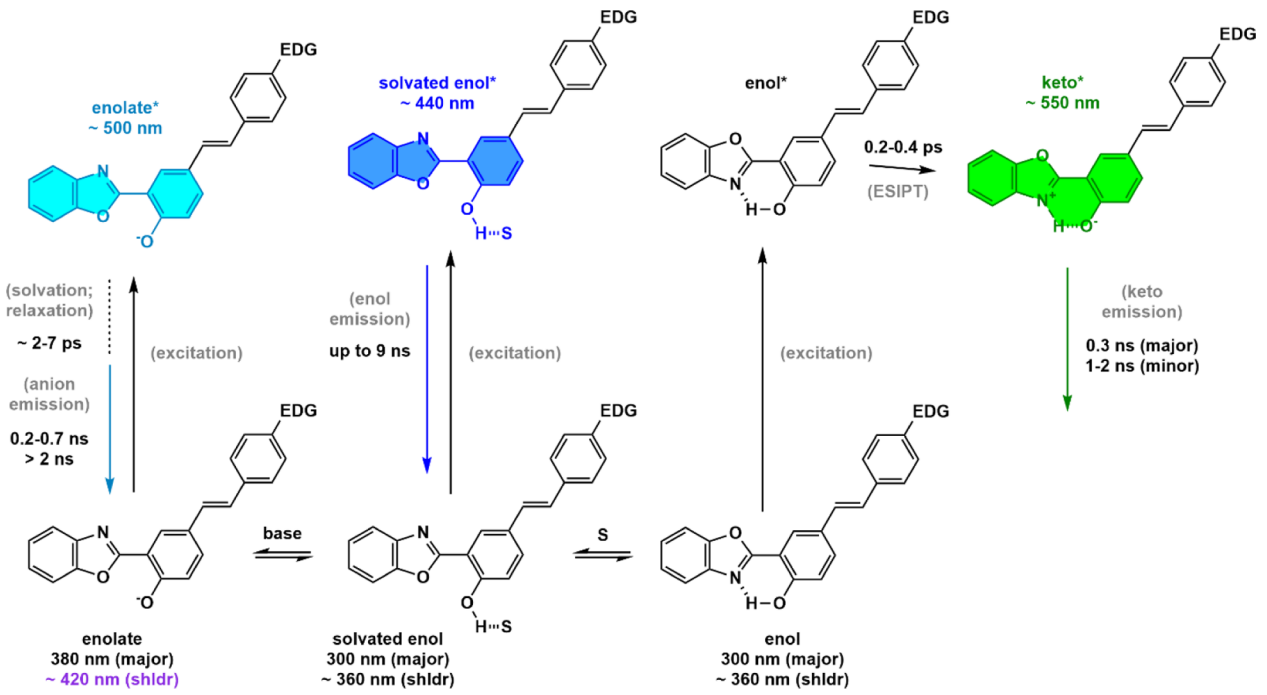

Figure 17. Structures that account for the emission properties of **PVHBO**s with an e-donating substituent (EDG). The LUMO component of an excited state is marked by the emission color of the respective species (the HOMO is invariably localized on the stilbenoid component at the S_0 geometries). The absorption and emission maxima (or shoulder) are listed and marked with a matching color when falling within the visible spectrum. The excited-state decays are noted next to the arrows.

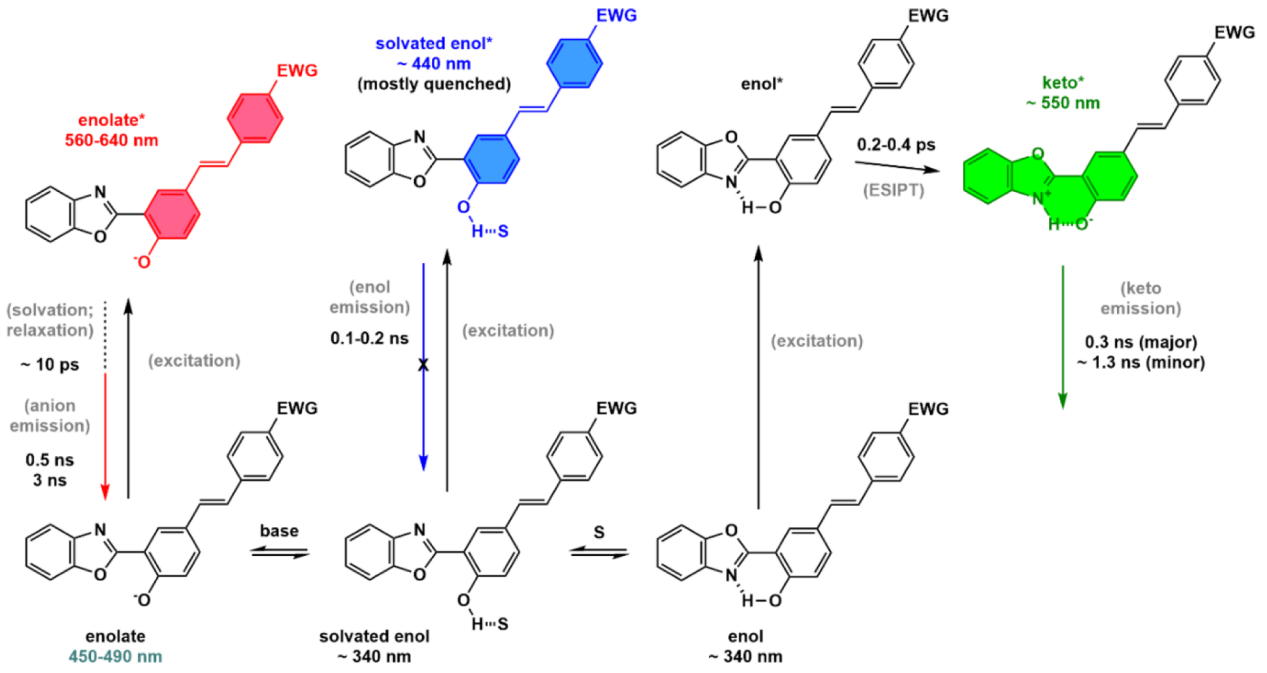

Figure 18. Structures that account for the emission properties of **PVHBO**s with an e-withdrawing substituent (EWG). The LUMO component of an excited state is marked by the emission color of the respective species (the HOMO is invariably localized on the stilbenoid component at the S_0 geometries). The absorption and emission maxima are listed and marked with a matching color when falling within the visible spectrum. The excited-state decays are noted next to the arrows.

absorption maxima of anions **1**−**5** coincide within a narrow range of the short wavelength region, while those of **6**−**10** are progressively longer as the R becomes more e-withdrawing (Figure 3).

Emission. The FMO dependence on the R group calculated at the S_1 geometries (Figure 16b) shows similarity to that at the S_0 geometries (Figure 16a), which explains the correlation between the emission maximum and the R group. The emission of group I anions, that is, the S_1 excitation energy calculated at the relaxed S_1 geometry, is dominated by the HOMO (alkoxide portion on stilbenoid) to LUMO (benzoxazole) transition (e.g., Figure 14a), which shows relative

https://doi.org/10.1021/acs.jpca.1c10167
J. Phys. Chem. A 2022, 126, 1062−1075

insensitivity to the R group (Figure 5). While for group II anions, the LUMO is located primarily at the R-substituted phenyl end of the stilbenoid (e.g., Figure 14b), thus giving rise to the sensitivity of group II anion emission to the R group. The localization of the fluorophoric component on a charge-transfer-type stilbenoid ("pushed" by the alkoxide and "pulled" by the e-withdrawing R group) could explain the dynamic Stokes shift of the SE captured in the fsTA data (e.g., Figure 10c), which is attributed to the solvent relaxation to accommodate the inversed dipole moment of the charge-transfer-type stilbenoid upon excitation.

Models That Summarize the Emission Properties of PVHBOs. The computational and time-resolved spectroscopic studies offer support to the following models that describe the emission properties of **PVHBO**s. When the R group is an e-donating group (EDG), the neutral fluorophore may exist with either an intramolecular HB, or an intermolecular HB with a solvent molecule. Both forms could be excited with photons of similar energy; while the former would undergo ESIPT to afford the green keto emission, the latter is the source of the enol emission in the blue region, as described in the preceding paper.[6] Upon deprotonation, the anion absorption moves into the visible blue region, while it emits near 500 nm.[14] The fluorescence decay of the anions bears more similarities to that of the solvated enol than the keto form, suggesting the closeness in the electronic structure of the excited anion and the solvated enol. All three excited-state species have similar FMO arrangements—the HOMO resides on the stilbenoid, while the LUMO occupies the HBO component as shown by the colors in Figure 17. Of the EDG-substituted **PVHBO**s, the absorption and emission spectra coincide in their respective spectral regions (see the values included in Figure 17), regardless of the nature of the substituent R.

The model that describes the emission behaviors of **PVHBO**s with an e-withdrawing substituent is shown in Figure 18. The space that the LUMO occupies in each excited species is marked by the color that matches the respective emission. The observations of the neutral species are listed in the preceding paper and are not repeated here. With an e-withdrawing substituent, the anion of a **PVHBO** behaves photophysically like a push−pull stilbenoid, on which both the HOMO and LUMO are found (at the S_0 geometry). The dynamic Stokes shift within 10 ps of excitation that is uniquely observed in the fsTA experiments is a consequence of the molecular dipole moment change of the charge-transfer stilbenoid fluorophore upon excitation.

Visible Spectrum Coverage by the Emission of PVHBOs. The unsubstituted HBO is capable of producing three emissive species—enol (E), anion (A), and keto (K). The E band centers at 370 nm in the UV region, while the A and K bands are found in blue to cyan regions of the visible spectrum—450 and 475 nm, respectively (red markers and line in Figure 19). When the 5′-position of HBO is substituted with an e-donating PV group to afford group I **PVHBO**s, all emission bands shift to longer wavelength regions, while the order of E, A, and K remains unchanged (Figure 19). DMSO drives the emission to the enol (E) band, while in DCM, only the keto (K) band is seen. When the 5′-position of HBO is substituted with an e-withdrawing PV group to afford group II **PVHBO**s, two major spectral changes occur: (1) the A band moves to a wavelength that is longer than those of both E and K bands. (2) The K band appears to be more abundant, even dominating in a HB-basic solvent such as DMSO. The latter, as described in the preceding paper, is attributed to the HB-mediated quenching of the enol emission of a group II **PVHBO**, which amplifies the K band.

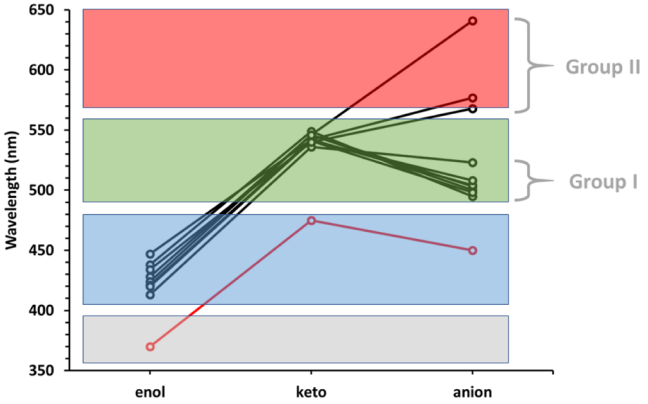

Figure 19. Sensitivities of enol, keto, and anion emission wavelengths of **PVHBO**s to the substituent R. As a reference, the respective values of unsubstituted HBO are 370, 475, and 450 nm as measured under identical conditions, which are shown as the red markers and line.

The sensitivity of the emission colors of **PVHBO**s to substituent R is plotted in Figure 19. The emission wavelengths of enol and keto forms are the averages of the values acquired in various solvents, while the anion emission wavelengths were measured in DMSO using DBU (20 molar equivalents) as the base. For differently substituted **PVHBO**s, neither the enol nor keto form is sensitive to substituent R. The former clusters in the blue region of the visible spectrum, while the latter peaks in the green section. On the contrary, the anion emission is sensitive to substituent R—an e-withdrawing R that is carried by each of the group II **PVHBO**s pushes the anion emission to a longer wavelength position than the neutral forms of both enol and keto emissions.

CONCLUSIONS

This article, together with the preceding one, offers a comprehensive account on the optical properties of 5′-PV-substituted 2-(2′-hydroxyphenyl)benzoxazoles (**PVHBO**s). These compounds can be considered as a fusion of two fluorophores—the ESIPT-capable HBO and the stilbenoid on the 5′-axis of the compound. Three emission bands can be produced, which are attributed individually to the enol, keto (the excited-state tautomer), and deprotonated anion species in the first singlet excited state. The emission wavelength maximum and the relative abundance of each band depend on both the solvent and the substituent R on the phenyl group. Depending on the nature of the R group, the studied compounds are separated into groups I (R is e-donating) and II (R is e-withdrawing). The keto emission of all **PVHBO**s results predominately from the intramolecularly bonded species (solvent-mediated ESIPT in EtOH is likely), whereas their abundances are maximized in non-hydrogen bonding solvents. The major distinctions between groups I and II compounds are revealed in the enol and anion emission properties in a hydrogen bonding solvent, such as DMSO. A group I compound affords the enol emission as the major component in DMSO, while the enol emission of a group II compound is quenched via strong hydrogen bonding with the solvent in the excited state. The anion emission of a group I compound exhibits insensitivity to the e-donating substituent R, while the energy of the emission of a group II anion

https://doi.org/10.1021/acs.jpca.1c10167
J. Phys. Chem. A 2022, 126, 1062−1075

decreases as the R becomes increasingly e-withdrawing. Fluorescent dyes capable of multiple emission have been studied in the context of and employed in an increasing volume of applications from bioimaging to energy-efficient illuminations. In this work, the dependencies on R and solvent of the multiple-emitting **PVHBO**s are explained by both ultrafast time-resolved spectroscopic observations and computational results, which yield predictive models that could correlate a structure to the emission color, relative abundance, and brightness of similar multiply-emitting dyes.

■ ASSOCIATED CONTENT

Supporting Information

The Supporting Information is available free of charge at https://pubs.acs.org/doi/10.1021/acs.jpca.1c10167.

Additional steady-state absorption and emission spectra; time-resolved absorption and emission spectra and kinetic decay traces; lifetimes and amplitude values extracted from time-resolved spectroscopic experiments; and computed data (PDF)

■ AUTHOR INFORMATION

Corresponding Author

Lei Zhu − *Department of Chemistry and Biochemistry, Florida State University, Tallahassee, Florida 32306-4390, United States;* orcid.org/0000-0001-8962-3666; Email: lzhu@fsu.edu

Authors

Joseph J. M. Hurley − *Department of Chemistry and Biochemistry, Florida State University, Tallahassee, Florida 32306-4390, United States*

Quinton J. Meisner − *Department of Chemistry and Biochemistry, Florida State University, Tallahassee, Florida 32306-4390, United States;* orcid.org/0000-0002-9342-0412

Peijun Guo − *Center for Nanoscale Materials, Argonne National Laboratory, Lemont, Illinois 60439, United States;* Present Address: Department of Chemical and Environmental Engineering, Yale University, 520 West Campus Drive, West Haven, CT 06516; orcid.org/0000-0001-5732-7061

Richard D. Schaller − *Center for Nanoscale Materials, Argonne National Laboratory, Lemont, Illinois 60439, United States;* orcid.org/0000-0001-9696-8830

David J. Gosztola − *Center for Nanoscale Materials, Argonne National Laboratory, Lemont, Illinois 60439, United States;* orcid.org/0000-0003-2674-1379

Gary P. Wiederrecht − *Center for Nanoscale Materials, Argonne National Laboratory, Lemont, Illinois 60439, United States*

Complete contact information is available at: https://pubs.acs.org/10.1021/acs.jpca.1c10167

Author Contributions

§J.J.M.H. and Q.J.M. contributed equally.

Notes

The authors declare no competing financial interest.

■ ACKNOWLEDGMENTS

This work was supported by the National Science Foundation (CHE1566011 and CHE1955262 to L.Z.). Use of the Center for Nanoscale Materials, an Office of Science user facility, was supported by the U.S. Department of Energy, Office of Science, Office of Basic Energy Sciences, under contract no. DE-AC02-06CH11357.

■ REFERENCES

(1) Kasha, M. Proton-Transfer Spectroscopy. *J. Chem. Soc., Faraday Trans. 2* **1986**, *82*, 2379−2392.

(2) Formosinho, S. J.; Arnaut, L. G. Excited-State Proton Transfer Reactions II. Intramolecular Reactions. *J. Photochem. Photobiol., A* **1993**, *75*, 21−48.

(3) Zhao, J.; Ji, S.; Chen, Y.; Guo, H.; Yang, P. Excited State Intramolecular Proton Transfer (ESIPT): from Principal Photophysics to the Development of New Chromophores and Applications in Fluorescent Molecular Probes and Luminescent Materials. *Phys. Chem. Chem. Phys.* **2012**, *14*, 8803−8817.

(4) Demchenko, A. P.; Tang, K.-C.; Chou, P.-T. Excited-State Proton Coupled Charge Transfer Modulated by Molecular Structure and Media Polarization. *Chem. Soc. Rev.* **2013**, *42*, 1379−1408.

(5) Zhou, P.; Han, K. Unraveling the Detailed Mechanism of Excited-State Proton Transfer. *Acc. Chem. Res.* **2018**, *51*, 1681−1690.

(6) Meisner, Q. J.; Hurley, J. J. M.; Guo, P.; Blood, A. R.; Schaller, R. D.; Gosztola, D. J.; Wiederrecht, G. P.; Zhu, L. Triple Emission of 5'-(para-R-Phenylene)vinylene-2-(2'-Hydroxyphenyl)benzoxazole (PVHBO). Part I: Dual Emission from the Neutral Species. *J. Phys. Chem. A*, **2022**. In press DOI: 10.1021/acs.jpca.1c10165.

(7) Abou-Zied, O. K.; Jimenez, R.; Thompson, E. H. Z.; Millar, D. P.; Romesberg, F. E. Solvent-Dependent Photoinduced Tautomerization of 2-(2'-Hydroxyphenyl)benzoxazole. *J. Phys. Chem. A* **2002**, *106*, 3665−3672.

(8) Yuan, Z.; Tang, Q.; Sreenath, K.; Simmons, J. T.; Younes, A. H.; Jiang, D.-e.; Zhu, L. Absorption and Emission Sensitivity of 2-(2'-Hydroxyphenyl)benzoxazole to Solvents and Impurities. *Photochem. Photobiol.* **2015**, *91*, 586−598.

(9) D'Andrade, B. W.; Forrest, S. R. White Organic Light-Emitting Devices for Solid-State Lighting. *Adv. Mater.* **2004**, *16*, 1585−1595.

(10) Kamtekar, K. T.; Monkman, A. P.; Bryce, M. R. Recent Advances in White Organic Light-Emitting Materials and Devices (WOLEDs). *Adv. Mater.* **2010**, *22*, 572−582.

(11) Bao, L.; Heagy, M. A Review of Single White-Light Emitters: The Quest for Picture Perfect Dyes in the Next Generation of Single Layer WOLED Displays. *Curr. Org. Chem.* **2014**, *18*, 740−772.

(12) Furche, F.; Ahlrichs, R.; Hättig, C.; Klopper, W.; Sierka, M.; Weigend, F. Turbomole. *Wiley Interdiscip. Rev.: Comput. Mol. Sci.* **2014**, *4*, 91−100.

(13) Meisner, Q. J.; Younes, A. H.; Yuan, Z.; Sreenath, K.; Hurley, J. J. M.; Zhu, L. Excitation-Dependent Multiple Fluorescence of a Substituted 2-(2′-Hydroxyphenyl)benzoxazole. *J. Phys. Chem. A* **2018**, *122*, 9209−9223.

(14) Hurley, J. J. M.; Meisner, Q. J.; Huang, C.; Zhu, L. Hydroxyaromatic Fluorophores. *ACS Omega* **2021**, *6*, 3447−3462.

(15) Devos, O.; Mouton, N.; Sliwa, M.; Ruckebusch, C. Baseline correction methods to deal with artifacts in femtosecond transient absorption spectroscopy. *Anal. Chim. Acta* **2011**, *705*, 64−71.

(16) Ruckebusch, C.; Sliwa, M.; Pernot, P.; de Juan, A.; Tauler, R. Comprehensive data analysis of femtosecond transient absorption spectra: A review. *J. Photochem. Photobiol., C* **2012**, *13*, 1−27.

(17) Sedgwick, A. C.; Wu, L.; Han, H.-H.; Bull, S. D.; He, X.-P.; James, T. D.; Sessler, J. L.; Tang, B. Z.; Tian, H.; Yoon, J. Excited-state intramolecular proton-transfer (ESIPT) based fluorescence sensors and imaging agents. *Chem. Soc. Rev.* **2018**, *47*, 8842−8880.

(18) Chen, W.-H.; Xing, Y.; Pang, Y. A Highly Selective Pyrophosphate Sensor Based on ESIPT Turn-On in Water. *Org. Lett.* **2011**, *13*, 1362−1365.

(19) Henary, M. M.; Wu, Y.; Fahrni, C. J. Zinc(II)-Selective Ratiometric Fluorescent Sensors Based on Inhibition of Excited-State Intramolecular Proton Transfer. *Chem.—Eur. J.* **2004**, *10*, 3015−3025.

(20) McMorrow, D.; Kasha, M. Intramolecular Excited-State Proton Transfer in 3-Hydroxyflavone. Hydrogen-Bonding Solvent Pertubations. *J. Phys. Chem.* **1984**, *88*, 2235−2243.
(21) Parthenopoulos, D. A.; Kasha, M. Ground State Anion Formation and Picosecond Excitation Dynamics of 3-Hydroxyflavone in Formamide. *Chem. Phys. Lett.* **1990**, *173*, 303−309.
(22) Sengupta, P. K.; Kasha, M. Excited State Proton-Transfer Spectroscopy of 3-Hydroxyflavone and Quercetin. *Chem. Phys. Lett.* **1979**, *68*, 382−385.
(23) McGarry, P. F.; Jockusch, S.; Fujiwara, Y.; Kaprinidis, N. A.; Turro, N. J. DMSO Solvent Induced Photochemistry in Highly Photostable Compounds. The Role of Intermolecular Hydrogen Bonding. *J. Phys. Chem. A* **1997**, *101*, 764−767.
(24) Nagaoka, S.-i.; Uno, H.; Huppert, D. Ultrafast Excited-State Intramolecular Proton Transfer of Aloesaponarin I. *J. Phys. Chem. B* **2013**, *117*, 4347−4353.
(25) Elsaesser, T.; Schmetzer, B. Excited-State Proton Transfer in 2-(2'-Hydroxyphenyl)benzothiazole: Formation of the Anion in Polar Solvents. *Chem. Phys. Lett.* **1987**, *140*, 293−299.
(26) Xu, L.; Wang, Q.; Zhang, Y. Electronic effect on the photophysical properties of 2-(2-hydroxyphenyl)benzothiazole-based excited state intramolecular proton transfer fluorophores synthesized by Sonogashira-coupling reaction. *Dyes Pigm.* **2017**, *136*, 732−741.

https://doi.org/10.1021/acs.jpca.1c10167
J. Phys. Chem. A 2022, 126, 1062−1075